Degradation of Pd/$Nb_{30}Ti_{35}Co_{35}$/Pd hydrogen permeable membrane

Journal of Membrane Science 601 (2020) 117922

Contents lists available at ScienceDirect

Journal of Membrane Science

journal homepage: http://www.elsevier.com/locate/memsci

Degradation of Pd/$Nb_{30}Ti_{35}Co_{35}$/Pd hydrogen permeable membrane: A numerical description

Xiao Liang [a], Xinzhong Li [a,b,*,1], Hiromi Nagaumi [b], Jingjie Guo [a], Fausto Gallucci [c], Martin van Sint Annaland [d], Dongmei Liu [e,**,1]

[a] School of Materials Science and Engineering, Harbin Institute of Technology, Harbin, 150001, PR China
[b] School of Iron and Steel, Soochow University, Suzhou, 215000, PR China
[c] Inorganic Membranes and Membrane Reactors, Department of Chemical Engineering and Chemistry, Eindhoven University of Technology, 5600, MB, Eindhoven, Netherlands
[d] Chemical Process Intensification, Department of Chemical Engineering and Chemistry, Eindhoven University of Technology, 5600, MB, Eindhoven, Netherlands
[e] Otto Schott Institute of Materials Research, Friedrich-Schiller-Universität, Jena, 07743, Germany

ARTICLE INFO

Keywords:
Pd/$Nb_{30}Ti_{35}Co_{35}$/Pd
Degradation
Hydrogen permeability
Aggregation
Interdiffusion

ABSTRACT

The hydrogen flux degradation in hydrogen permeation tests of Pd/$Nb_{30}Ti_{35}Co_{35}$ (at.%)/Pd composite membranes was experimentally investigated at temperatures from 400 to 650 °C. The hydrogen fluxes through the Pd/$Nb_{30}Ti_{35}Co_{35}$/Pd membranes during isothermal long-term hydrogen permeation tests above 500 °C exhibit two hydrogen-flux-decline steps. The aggregation of the Pd-catalytic layer and the boundary layer formed between Pd and $Nb_{30}Ti_{35}Co_{35}$ due to interdiffusion were experimentally confirmed contributing to the degradation of the hydrogen flux through the Pd/$Nb_{30}Ti_{35}Co_{35}$/Pd membrane. Modelling work was carried out to reveal and validate the temperature-dependence of the two attributing factors to the degradation of hydrogen permeation flux.

1. Introduction

The increasing demand for high-purity hydrogen (>99.999%) as a clean energy carrier for LED and fuel cell applications is inspiring interest in developing technologies for more efficient high-purity hydrogen production [1]. Membrane technology, which purifies lower-purity hydrogen obtained by water-gas-shift or gas reforming from fossil fuel to hydrogen of the desired high-purity, plays a critical role [2–7]. Palladium (Pd)-based membranes are intensively used for hydrogen purification due to their high selectivity, high hydrogen permeability, and excellent chemical compatibility [4–6,8]. The main drawback of Pd-alloy membranes is the high cost. Research on the design of Pd-alloy membrane of ever-decreasing thickness and on the development of alloy membranes containing little or no Pd is on-going [9–11]. Body-centred-cubic (BCC) group 5 metals (V, Nb and Ta) are considered as promising substitutions because of their high hydrogen permeability [12–14]. For improving the mechanical stability of group 5 metals, alloyed BCC metals [15,16] and dual-phase alloys consisting of BCC phase in a matrix of an eutectic structure [14–17] have been developed, which exhibit enhanced resistance to the hydrogen embrittlement.

For further improvement of hydrogen permeability and mechanical stability, higher application temperature of the group 5 alloy membranes is preferred, considering reduced hydrogen solubility and increased hydrogen diffusivity with increasing temperature [18]. This can also solve the dilemma in high-purity hydrogen production industry, where a temperature reduction procedure between the low-purity hydrogen generation and the following hydrogen purification of higher purity is needed because of the higher operating temperature of the former step (>500 °C) and the relatively lower working upper limit of the membrane in the latter step (≤400 °C for stable operation) [19]. However, the higher operating temperature strategy is challenging for group 5 alloys membrane. For dissociation and absorption of hydrogen molecules during purification, Pd catalytic layers and Pd coated membranes, as e.g. Pd/Nb–Ti–Co/Pd composite membranes, are generally used. When the operating temperature is higher than 400 °C,

* Corresponding author. School of Materials Science and Engineering, Harbin Institute of Technology, Harbin, 150001, PR China.
** Corresponding author.
E-mail addresses: lixz@suda.edu.cn (X. Li), dongmei.liu@uni-jena.de (D. Liu).
[1] These authors contributed equally to this work.

https://doi.org/10.1016/j.memsci.2020.117922
Received 19 November 2019; Received in revised form 31 January 2020; Accepted 3 February 2020
Available online 3 February 2020

interdiffusion between the Pd catalytic layer and the substrate alloys occurs, which leads to degradation of hydrogen flux [20]. In recent years, investigations on the formation of the intermediate layer of low hydrogen permeability [21,22], and the formation of pinholes and cracks in the Pd catalytic layer [23] started. These findings shed a light on the necessity of theoretical study on the interdiffusion between substrate and Pd-coating layers and on the following optimization of membrane structure.

In the present work, $Nb_{30}Ti_{35}Co_{35}$ (at.%) alloy, which is characterized by fully eutectic structure, BCC-(Nb, Ti) and B2-(Ti, Co) [24,25] and thus of good mechanical stability during operation, is chosen as the substrate alloy. The Pd/$Nb_{30}Ti_{35}Co_{35}$/Pd composite membranes were reported to exhibit hydrogen permeability of 2.67×10^{-8} mol H_2 m^{-1} s^{-1} $Pa^{-0.5}$ for isotropic eutectic lamellae structure and 4.26×10^{-8} mol H_2 $m^{-1}s^{-1}Pa^{-0.5}$ for aligned eutectic lamellae structure at 400 °C [24,25]. In the present work, the stability of hydrogen permeability of the Pd/$Nb_{30}Ti_{35}Co_{35}$/Pd composite membrane during hydrogen permeation test at temperatures above 400 °C has been analyzed. A model for predicting the hydrogen flux during long-term hydrogen permeation test has been proposed, which correlates the change in membrane structure and its hydrogen permeability during the permeation process at different temperatures. This provides information for selection of pertinent membrane materials and suitable operating temperatures for effective hydrogen purification.

2. Experiments and modelling

Ingots of ~35g of $Nb_{30}Ti_{35}Co_{35}$ were prepared by arc melting under high purity Ar (99.999%) atmosphere from Nb, Ti and Co elements (99.9 purity for all). All ingots were turned over and remelted for 6 times to ensure macro-scale homogeneous composition. Disks of the diameter of 16 mm were cut from the ingot by spark erosion wire-cutting. Both sides of the disks were mechanically ground and polished, and the final thickness was controlled as 0.6 mm. Subsequently, the catalytic layer of pure Pd was deposited at each side of the disk by radio frequency magnetron sputtering (ZC-1000). The sputtering process was performed at 300 °C under high purity Ar atmosphere. The working power was 0.4 kW and the sputtering distance was 60 mm. The pressure at the backside and the working side was 2×10^{-4} and 0.5 Pa, respectively. The sputtering process lasted 150 s, and the thickness of the Pd catalytic layer was aimed as 1 μm. The microstructure of the Pd/$Nb_{30}Ti_{35}Co_{35}$/Pd composite membrane was analyzed using scanning electron microscopy (SEM - FEI Quanta 200FEG) equipped with energy dispersive spectrometer (EDS - EDAX). This includes the surface morphology, the thickness of the Pd layer, and the microstructure/composition across the Pd/$Nb_{30}Ti_{35}Co_{35}$ interfaces. The constituent phases of the Pd/$Nb_{30}Ti_{35}Co_{35}$/Pd composite membranes before and after hydrogen permeation tests were characterized using the X-ray diffraction analysis (XRD- Rigaku MiniFlex 600) equipped with Cu-Kα radiation by the step rate of 0.1°/min (with the step size of 0.02°) in 2θ range of 20–100°.

The hydrogen permeation behavior of Pd/$Nb_{30}Ti_{35}Co_{35}$/Pd membrane was characterized using in-house gas permeation setup. Disk samples were sandwiched and fixed between two copper gaskets and sealed in the hydrogen permeation setup. The two sides of the membrane were evacuated and heated up to the target temperature (400, 450, 500, 550, 600, and 650 °C) at a heating rate 5 °C/min and stabilized for 30 min under vacuum. Subsequently, pure H_2 (99.999%) was introduced into the upstream side and the downstream side until 0.1 MPa. Then, the H_2 pressure at the upstream side was increased to 0.7 MPa step by step. At the same time, the H_2 pressure at the downstream side was kept at 0.1 MPa. The hydrogen flux through the membrane was measured with a H_2 mass flow meter (Alicat MS-20 sccm). After the hydrogen permeation test, both the upstream and downstream were evacuated, and then the heating system was turned off. More details about the hydrogen permeation test can be found in the previous work [24–26]. For characterizing the stability of hydrogen flux through Pd/$Nb_{30}Ti_{35}Co_{35}$/Pd membranes, hydrogen permeation tests up to 330 h with the upstream H_2 pressure of 0.7 MPa were performed, during which the hydrogen flux was recorded. A decline of hydrogen flux was observed during long-term tests. Hence, identical tests but of different durations were performed. This aims to investigate the morphological evolution of the Pd/$Nb_{30}Ti_{35}Co_{35}$/Pd membranes during the long-term hydrogen permeation process. In the present work, a series of Pd/$Nb_{30}Ti_{35}Co_{35}$/Pd membranes produced by the identical process, including as-cast $Nb_{30}Ti_{35}Co_{35}$ ingot preparation and the sputtering process, were used. A new membrane was used for each test mentioned above. The surface microstructure of the Pd layer and the microstructure of the cross section of Pd/$Nb_{30}Ti_{35}Co_{35}$/Pd membranes after hydrogen permeation tests were characterized by SEM-EDS. Linear EDS analysis across the Pd/$Nb_{30}Ti_{35}Co_{35}$ interface was performed with a step interval of 50 nm, aiming to analyze the interdiffusion between the Pd catalytic layer and $Nb_{30}Ti_{35}Co_{35}$ substrate during the hydrogen permeation at high temperatures.

The interdiffusion between the Pd and the substrate was considered as simple diffusion couple. A self-designed model using the COMSOL Multiphasic Modeling Software was applied to analyze the influence of Pd distribution on the hydrogen flux through the Pd/$Nb_{30}Ti_{35}Co_{35}$/Pd membrane. In the model, the difference in hydrogen diffusion between the Pd layer and the $Nb_{30}Ti_{35}Co_{35}$ substrate, the reaction between hydrogen and materials resulting in solution of hydrogen into the material, and the transport of hydrogen through the material were considered.

3. Result and discussion

3.1. Hydrogen permeation tests

The microstructure of the Pd/$Nb_{30}Ti_{35}Co_{35}$/Pd membrane and the composition distribution across the Pd/$Nb_{30}Ti_{35}Co_{35}$ interface before the hydrogen permeation test are shown in Fig. 1. A dense and intact Pd coating layer of thickness of 1 μm was confirmed after the sputtering process, as shown in Fig. 1(a). Beneath the Pd layer, the fully lamellar eutectic structure was confirmed for the $Nb_{30}Ti_{35}Co_{35}$ substrate, as shown in Fig. 1(b). The Pd/$Nb_{30}Ti_{35}Co_{35}$ interface is sharp, and there is no microstructural and compositional change (Fig. 1(c)) in the substrate $Nb_{30}Ti_{35}Co_{35}$ beneath the Pd layer. This is further confirmed by the linear composition analysis across the Pd/$Nb_{30}Ti_{35}Co_{35}$ interface. It is not straightforward to separate the four elements involved, hence, a deviation of Pd from 100% in the Pd layer and a deviation of Nb/Ti/Co from the nominal composition of $Nb_{30}Ti_{35}Co_{35}$ exist.

The hydrogen flux through the Pd/$Nb_{30}Ti_{35}Co_{35}$/Pd membranes during long-term hydrogen permeation tests at different temperatures is shown in Fig. 2. During the hydrogen permeation process, the hydrogen pressure at the upstream side, P_u, was maintained as 0.7 MPa, and that at the downstream side, P_d, as 0.1 MPa. During the hydrogen permeation test at 400 °C, the hydrogen flux maintained constant as 17.5×10^{-3} mol H_2 m^{-2} s^{-1} (calculated hydrogen permeability of 21×10^{-6} mol H m^{-1} s^{-1}) up to 330 h. For the tests at 450–650 °C, degradation of the hydrogen flux was observed. The degradation rate increases with increasing temperature. At 450 °C, the hydrogen flux decreases to 90% of the initial value after 330 h. It is worth noting that the initial hydrogen flux at 450 °C is higher than that at 400 °C, which indicates the positive effect of increasing operating temperature on hydrogen flux and thus the working efficiency of the membrane. Resulting from the higher hydrogen flux at 450 °C, the hydrogen flux at 450 °C after 330 h is still higher than that at 400 °C. These results indicate a higher working efficiency of the Pd/$Nb_{30}Ti_{35}Co_{35}$/Pd membrane at 450 °C for hydrogen separation than that at 400 °C. However, for evaluation of optimal operating temperature, a further determination of hydrogen flux after longer hydrogen permeation durations is still needed. Although the initial hydrogen flux at 500 °C is even higher, the fast degradation rate results in much lower hydrogen flux after 330 h. For tests at 550 … 650

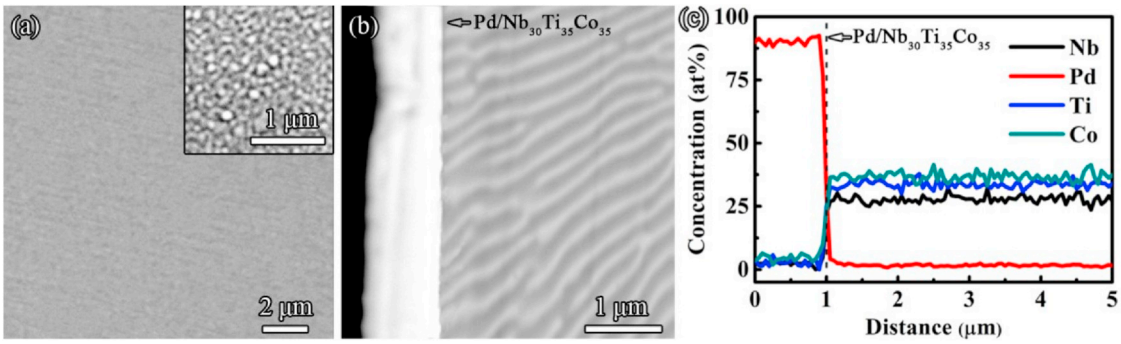

Fig. 1. (a) Backscattered electron (BSE) images of the surface Pd catalytic layer; (b) Pd/$Nb_{30}Ti_{35}Co_{35}$ interface from the cross section; (c) composition profile across the Pd/$Nb_{30}Ti_{35}Co_{35}$ interface.

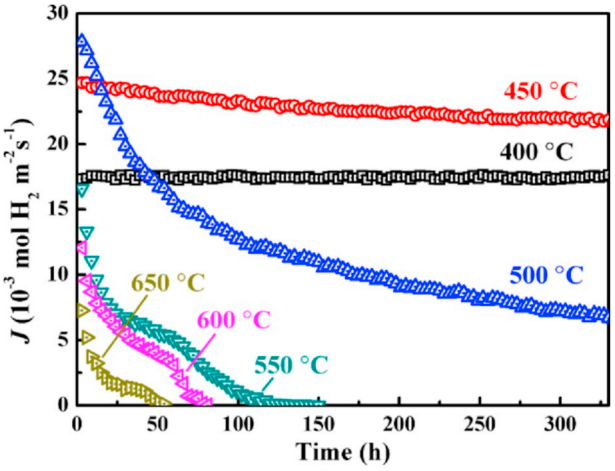

Fig. 2. Hydrogen flux (J) through the Pd/$Nb_{30}Ti_{35}Co_{35}$/Pd membrane during long-term hydrogen permeation tests at 400 … 650 °C, during which the upstream hydrogen pressure P_u is maintained as 0.7 MPa, and that at the downstream side P_d is 0.1 MPa.

°C, the hydrogen flux decreases to zero in a short time, which indicates serious deterioration of the Pd/$Nb_{30}Ti_{35}Co_{35}$/Pd membrane at the beginning with operating temperatures above 500 °C, and then the degradation rate becomes slower with increasing duration. At 550 … 650 °C, after a short plateau, the degradation becomes faster again until the complete failure. This is probably related to the different degradation mechanisms, which will be discussed later in the present work.

For figuring out the reason for the hydrogen flux degradation, permeation tests of identical temperature and hydrogen pressure but of various test durations were performed. After the hydrogen permeation test, the surface morphology of Pd layers and the microstructure across the Pd/$Nb_{30}Ti_{35}Co_{35}$ interfaces at the upstream side and the downstream side are similar. This indicates that the microstructure change of the surface Pd layer and the interdiffusion between the Pd layer and the $Nb_{30}Ti_{35}Co_{35}$ substrate are not sensitive to the H_2 partial pressure, i.e. H concentration in the material. The microstructure of the membrane surface at the upstream side is shown in Fig. 3. The Pd layer after the test at 400 and 450 °C for 330 h, coarsening of the Pd layer was observed, as shown in Fig. 3(a), (b), but no penetrate defects were found, and the Pd coverage was still 100%. According to the XRD analysis (Fig. 3(g)) and the composition analysis of the surface layer, the surface layer after tests at 400 and 450 °C was still pure Pd. When the hydrogen permeation temperature increased up to 500 °C (Fig. 3(c)), serious damage of the Pd layer after 330 h occurred, and only part of the $Nb_{30}Ti_{35}Co_{35}$ substrate was covered by Pd. This might lead to deteriorated hydrogen dissociation at the upstream side. According to the XRD analysis, $TiPd_x$ (x = 1, 2, 3) phase, BCC-Nb and B2 phase (TiCo) from the substrate were detected besides pure Pd, indicating the thinning of the surface Pd layer. With further increase of the test temperature to 550 °C (Fig. 3(d)), even after a shorter test duration of 150 h, the coverage of Pd decreased seriously. By relating to XRD results, the main diffraction peak of Pd was much weaker than the original state and the peaks of $TiPd_x$ phase became strong, indicating the fast formation of $TiPd_x$ at the surface at 550 °C. After the test at 600 °C for 80 h, grains of the $Nb_{30}Ti_{35}Co_{35}$ substrate were clearly visible, as shown in Fig. 3(e), indicating nearly total loss of the Pd layer, which was consistent with the XRD analysis. This was supposed to be the main reason for nil hydrogen flux at 600 °C after 80 h (Fig. 2). After hydrogen permeation at 650 °C for 60 h, the Pd layer disappeared totally, resulting in nil hydrogen permeation flux. In summary, during the long-term hydrogen permeation test at 500 … 650 °C, with increasing operating duration, the Pd coating layer became thinner and thinner, resulting in loss of catalytic effect of Pd for dissociation of hydrogen. Besides, $TiPd_x$ formed due to the interdiffusion between the substrate and the Pd coating layer, which behaved as a barrier for hydrogen permeation and resulted in sluggish diffusion of hydrogen through the membrane. These two factors led to the fast reduction of the hydrogen flux through the membrane.

For characterizing the interdiffusion between the Pd catalytic layer and the $Nb_{30}Ti_{35}Co_{35}$ substrate, permeation tests of identical temperature and hydrogen pressure but of various test durations were performed using a series of Pd/$Nb_{30}Ti_{35}Co_{35}$/Pd membranes. The evolution of the surface Pd layer and composition across the Pd/$Nb_{30}Ti_{35}Co_{35}$ interface during the hydrogen permeation test are shown in Fig. 4. At 450 °C, with increasing test duration, grooves between Pd grain boundaries formed and became deeper. However, the coverage of the Pd layer was still 100% after 330 h. In the present work, the initial thickness of the Pd layer is 1 μm. In such situation, the rate of hydrogen transport through the Pd layer is controlled by surface reaction, i.e. dissociation and association of H_2 molecules at the upstream and downstream sides [27, 28]. According to the work of Al-Mufachi et al. [4], a slightly defected Pd layer consisting of grooves as in Fig. 4(d) exhibits an even higher hydrogen dissociation rate due to the increase of the surface area and the activated positions for dissociation. This means that other reason(s) than the morphology change of the Pd layer should be responsible for the degraded hydrogen flux. The analysis of the composition profile across the Pd/$Nb_{30}Ti_{35}Co_{35}$ interface, as shown in Fig. 4(h), confirmed the interdiffusion between the Pd layer and the $Nb_{30}Ti_{35}Co_{35}$ substrate during the long–term hydrogen permeation test at 450 °C. In comparison with abrupt composition change across the Pd/$Nb_{30}Ti_{35}Co_{35}$ interface, a transition layer appeared below the surface Pd-coating layer, where the Pd concentration reduced slowly from ~100% to 0%. This layer formed as a result of the interdiffusion between the Pd layer and the $Nb_{30}Ti_{35}Co_{35}$ substrate. The thickness of the boundary layer increased from 0.3 μm after 24 h test to 1.2 μm after 330 h. When the temperature of the hydrogen permeation process reached up to 550 °C, grooving and deterioration in the morphology of the Pd layer occurred much faster, as shown in Fig. 4(e and f). Besides the clustering of Pd,

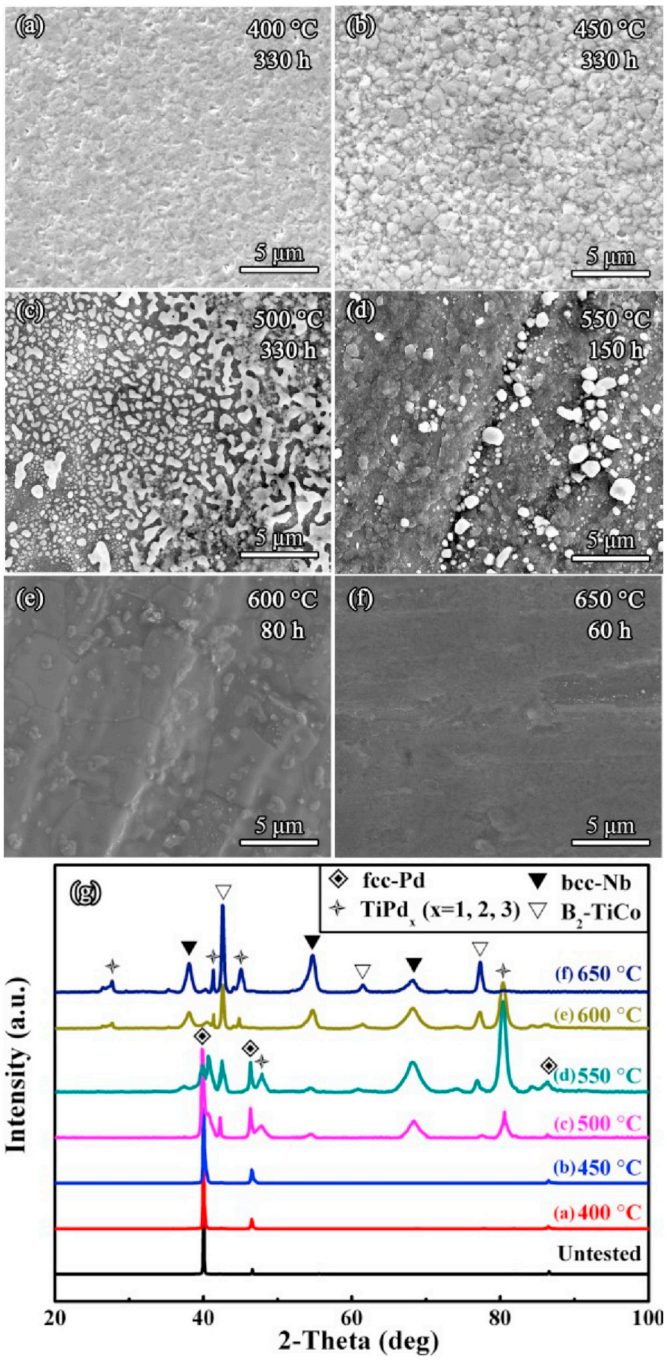

Fig. 3. BSE images (a–f) and XRD patterns (g) of the surface layer of Pd/$Nb_{30}Ti_{35}Co_{35}$/Pd membranes after hydrogen permeation tests.

pinholes in surface layer formed, leading to a fast reduction of the coverage of the Pd on the $Nb_{30}Ti_{35}Co_{35}$ substrate. The coverage of the Pd layer decreased to 74% in 48 h, and a total loss of the Pd layer occurred after 150 h. The average gap between the Pd particles was characterized statistically using the software Image pro plus 6.0. The gap first increased slowly, and after reaching 1 μm at 72 h, it started to increase rapidly to 11 μm at 150 h. This led to a highly reduced dissociation rate of hydrogen molecule to hydrogen atoms at the Pd interface, which resulted in the fast deterioration of hydrogen flux. This is consistent with the experimental observation (Fig. 2), where a fast degradation rate of hydrogen flux occurs after 72 h hydrogen permeation at 550 °C.

Judging from the composition profile across the Pd/$Nb_{30}Ti_{35}Co_{35}$ interface (Fig. 4(i)), the interdiffusion between Pd and $Nb_{30}Ti_{35}Co_{35}$ at 550 °C occurred much faster than that at 500 °C. After a 12 h hydrogen permeation test at 550 °C, there is no pure Pd layer at all and a boundary layer of 1.75 μm forms. With further proceed of the hydrogen permeation, the thickness of the boundary layer increases up to 2.5 μm after 48 h and more than 5 μm after 150 h. It is worth noting that after 150 h, the total amount of Pd in the membrane is lower than the initial value, indicating the peeling of the Pd layer. With further increase of the operating temperature of the membrane, the interdiffusion and the deterioration of the Pd layer are supposed to occur much faster, which leads to a faster drop of the hydrogen flux to zero in a short operating duration, as demonstrated by Fig. 2.

3.2. Modelling

Based on the experimental observation, the degradation of the hydrogen permeability results from two factors: (1) the aggregation of the Pd catalytic layer, and (2) the formation of the boundary layer at the Pd/$Nb_{30}Ti_{35}Co_{35}$ interface resulting from the interdiffusion between the Pd catalytic layer and the $Nb_{30}Ti_{35}Co_{35}$ substrate. Combining the boundary factor ($f_b(t)$) and the Pd aggregation factor ($f_{Pd}(t)$), the degradation of the hydrogen flux during long-term permeation tests at high operating temperatures can be described as,

$$J = J_0 \cdot f_b(t) \cdot f_{Pd}(t) \quad (1)$$

where t is the time, J is the real-time hydrogen flux, J_0 is the hydrogen flux at the start of the test, which is assumed to be the ideal hydrogen flux through the Pd/$Nb_{30}Ti_{35}Co_{35}$/Pd membrane at a certain temperature and a certain hydrogen pressure drop between the upstream and downstream sides.

For simplification, the influences of the Pd/$Nb_{30}Ti_{35}Co_{35}$ boundary layer and the Pd aggregation on the degradation of hydrogen flux were considered separately. When considering the boundary factor, it is assumed that: (1) the permeation through the Pd layers at the upstream and downstream sides is limited by hydrogen adsorption and desorption respectively, and $f_{Pd}(t) = 100\%$; (2) the hydrogen permeation through the Pd/$Nb_{30}Ti_{35}Co_{35}$/Pd membrane is controlled by the hydrogen diffusion through the $Nb_{30}Ti_{35}Co_{35}$ layer; and that (3) the boundary layer exhibits constant hydrogen solubility and diffusivity across the whole boundary layer.

At the beginning of the hydrogen permeation process, the Pd catalytic layer is compact and there is no boundary layer between the Pd layer and the $Nb_{30}Ti_{35}Co_{35}$ substrate, as shown in Fig. 5(a). The thickness of the $Nb_{30}Ti_{35}Co_{35}$ layer is denoted as l_{Nb} and the thickness of the Pd layer is denoted as l_{Pd}. When the hydrogen permeation through the membrane reaches the steady state, the concentration of H at the upstream side is:

$$c_u = K_{Nb} P_u^{0.5} \quad (2)$$

At the downstream side, the H concentration is:

$$c_d = K_{Nb} P_d^{0.5} \quad (3)$$

where K_{Nb} is the Sievert's constant of $Nb_{30}Ti_{35}Co_{35}$, P_u is the hydrogen pressure at the upstream surface, and P_d is the hydrogen pressure at the downstream surface. In the present work, the lower case, Pd, Nb, and b stand for the Pd layer, the $Nb_{30}Ti_{35}Co_{35}$ layer and the boundary layer at the Pd/$Nb_{30}Ti_{35}Co_{35}$ interface. When the interdiffusion between the Pd layer and the $Nb_{30}Ti_{35}Co_{35}$ substrate occurs, the boundary layer forms between the Pd layer and $Nb_{30}Ti_{35}Co_{35}$ substrate, and the interfaces from the upstream surface to the downstream surface are defined as interface 0 to 5, as shown in Fig. 5(b).

The growth of the boundary layer can be described as [29–31]:

$$l_b = \gamma\sqrt{t} \quad (4)$$

where l_b is the thickness of the boundary layer, γ is the coefficient of

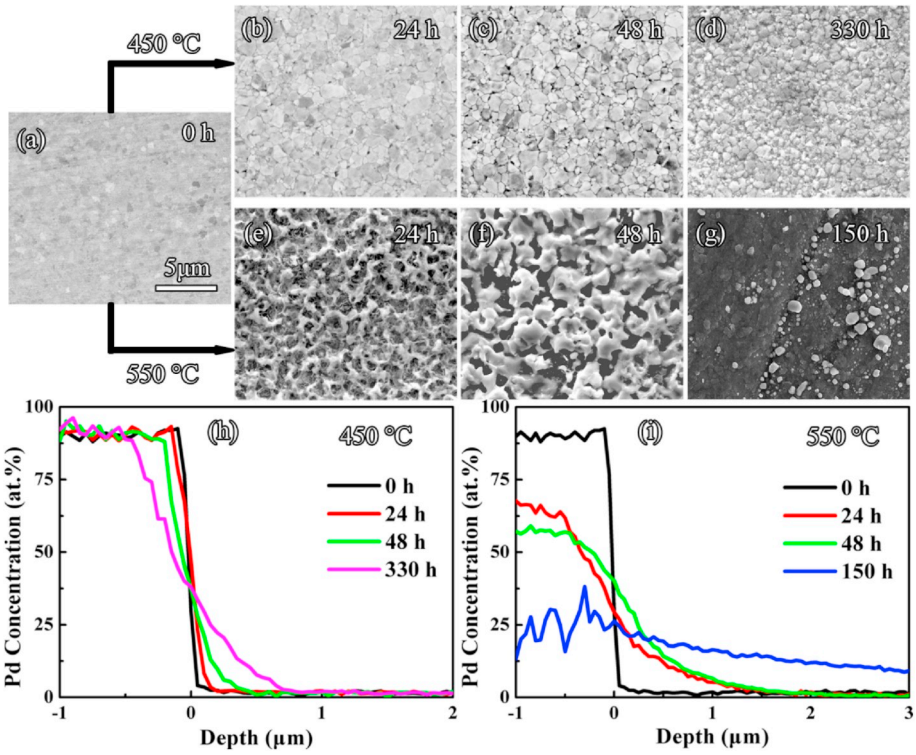

Fig. 4. Surface Pd layer morphology after hydrogen permeation test at 450 and 550 °C (a–g), and the linear EDS analysis of the composition across the Pd/$Nb_{30}Ti_{35}Co_{35}$ interface at the cross section (h), (i).

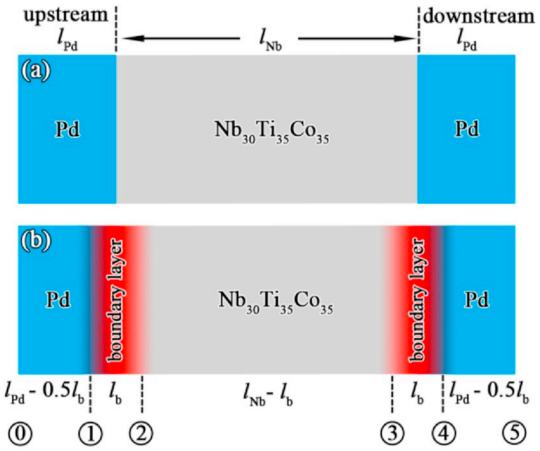

Fig. 5. Schematic illustration of the hydrogen permeation through the multi-layer Pd/$Nb_{30}Ti_{35}Co_{35}$/Pd membrane;
(a) no Pd/$Nb_{30}Ti_{35}Co_{35}$ boundary layer; (b) formation of boundary layers at Pd/$Nb_{30}Ti_{35}Co_{35}$ interface.

diffusion couple between Pd and $Nb_{30}Ti_{35}Co_{35}$, and t is time.

According to the previous work [32], the hydrogen flux through a multilayer membrane can be calculated as:

$$J = \frac{P_u^{0.5} - P_d^{0.5}}{\sum_i \frac{l_i}{K_i D_i}} \tag{5}$$

where l_i is the thickness of i-layer, K_i is the hydrogen solubility constant of i-layer, and D_i is the hydrogen diffusion coefficient of i-layer.

Correlating the Appendix, taking the influence of the boundary layer into consideration, the time dependency of the hydrogen flux during long term permeation tests can be described as:

$$f_i(t) = \frac{1}{1 + \beta\sqrt{t}} \tag{6}$$

where β is the influence factor resulting from the interdiffusion between the Pd and $Nb_{30}Ti_{35}Co_{35}$.

$$\beta = \frac{2\gamma}{K_b D_b} \times \frac{K_{Nb} D_{Nb}}{l_{Nb}} \tag{7}$$

where K_b is the hydrogen solubility constant of the boundary layer, and D_b and D_{Nb} are the hydrogen diffusivities of the boundary layer and $Nb_{30}Ti_{35}Co_{35}$, respectively.

When the operating temperature is beyond 500 °C, the aggregation of the Pd layer occurs, as shown in Figs. 3 and 4. For incorporating the influence factor resulting from Pd aggregation, the transport of hydrogen through the Pd/$Nb_{30}Ti_{35}Co_{35}$/Pd composite membrane with different Pd cover patterns was first calculated based on a two-dimensional calculation. During such calculation, the interdiffusion between the Pd and $Nb_{30}Ti_{35}Co_{35}$, the resulted boundary layers and their influence on the hydrogen flux are neglected for simplification. The dissociation of H_2 to H atoms at the upstream side and the association H atoms to H_2 at the downstream side are closely related to the integrity and the effective integral surface of Pd coating layers, as e.g. the coverage ratio of Pd layer on the surface of $Nb_{30}Ti_{35}Co_{35}$ substrate. In the present model, the diameter of the Pd particle in the cross section is denoted as d and the spacing between two Pd particles is denoted as g.

The diffusion of hydrogen through the membrane follows the solution-diffusion mechanism [33], and the concentration variation is calculated based on the Fick's law and the mass conservation:

$$\frac{\partial c}{\partial t} = \nabla(D\nabla c) + R \tag{8}$$

where c is the concentration of hydrogen in the membrane (mol H/m^3), D is the diffusion coefficient of hydrogen (m^2/s), and R is the reaction rate for hydrogen (mol H/(m^3·s)).

For the steady hydrogen diffusion through the membrane, the concentration of hydrogen at the surfaces of the upstream side (c_u) and downstream side (c_d) of the $Nb_{30}Ti_{35}Co_{35}$ substrate layer are assumed as 3.5 and 2.0 × 10^4 mol H/m^3, respectively, based on our previous work on the Pd/$Nb_{30}Ti_{35}Co_{35}$/Pd membranes [33]. Diffusion coefficients of hydrogen in Pd and $Nb_{30}Ti_{35}Co_{35}$, $D_{Pd} = 5.77 \times 10^{-9}$ m^2/s [34,35], $D_{Nb} = 4.76 \times 10^{-10}$ m^2/s [33], are used. The flux vector N is defined as Eq. (9).

$$N = -D\nabla c \tag{9}$$

For characterizing the influence of the Pd aggregation on the hydrogen flux, the dissociation of H_2 to H atoms on the surface of the Pd layer at the upstream side and the association of H atoms to H_2 at the downstream side are correlated with the Pd catalytic layers. Not only the coverage ratio of the Pd layer (i.e. the effective integral surface of Pd for hydrogen permeation) but also the distribution of the Pd particles are considered, as shown in Fig. 6. The isolines in Fig. 6 (d) ~ (i), from red to blue, stand for the hydrogen concentration from c_u(=3.5 × 10^4 mol H/m^3) to c_d (=2.0 × 10^4 mol H/m^3) with a constant interval of 1 × 10^4 mol H/m^3. With Pd coverage of 100% (Fig. 6(b)), the homogenous distribution of the isolines perpendicular to the permeation direction is reached, indicating only one hydrogen flux vector, and the hydrogen flux reaches the ideal value of $Nb_{30}Ti_{35}Co_{35}$. With reduced coverage ratio of 50% and $g = d$ =1, 2, 5 μm, as shown in Fig. 6 (c)–(e), the hydrogen flux can also reach approximately 100% of the ideal value. However, with the same Pd coverage of 50%, increasing size of Pd particles up to 100 μm leads to drop of hydrogen flux down to 93.77%, as shown in Fig. 6 (f)–(i). This indicates that besides the Pd coverage, the distribution of Pd particles plays a critical role in the permeation of hydrogen through the Pd/$Nb_{30}Ti_{35}Co_{35}$/Pd membranes, as demonstrated by the H isolines across the membrane.

Considering the two dimensional distribution of Pd particle on the membrane surface, three-dimensional (3D) calculations were performed to investigate the influence of Pd aggregation on the hydrogen flux through the Pd/$Nb_{30}Ti_{35}Co_{35}$/Pd membrane, as shown in Fig. 7. For simplification, the Pd particles during the hydrogen permeation, even after the aggregation, are assumed uniformly distributed in the shape of a cylinder, as illustrated in Fig. 7 (a). The thickness of the $Nb_{30}Ti_{35}Co_{35}$ substrate and the Pd layer is set as 600 μm and 1 μm respectively. For demonstrating the influence of Pd distribution on the H distribution across the membrane and the resulted hydrogen permeation, a Pd particle diameter, d = 50 μm, and a gap between the Pd particles, g = 25 μm, were chosen, as shown in Fig. 7(b). A single unite during calculation is shown in Fig. 7(c). The initial hydrogen concentration at the upstream and downstream sides, c_u and c_d, are 3.5 × 10^4 and 2.0 × 10^4 mol H/m^3 respectively. Using COMSOL, the hydrogen concentrate distribution through the membrane was obtained, as shown in Fig. 7(d). The isosurfaces in Fig. 7(d) of colors from red to blue stand for the hydrogen

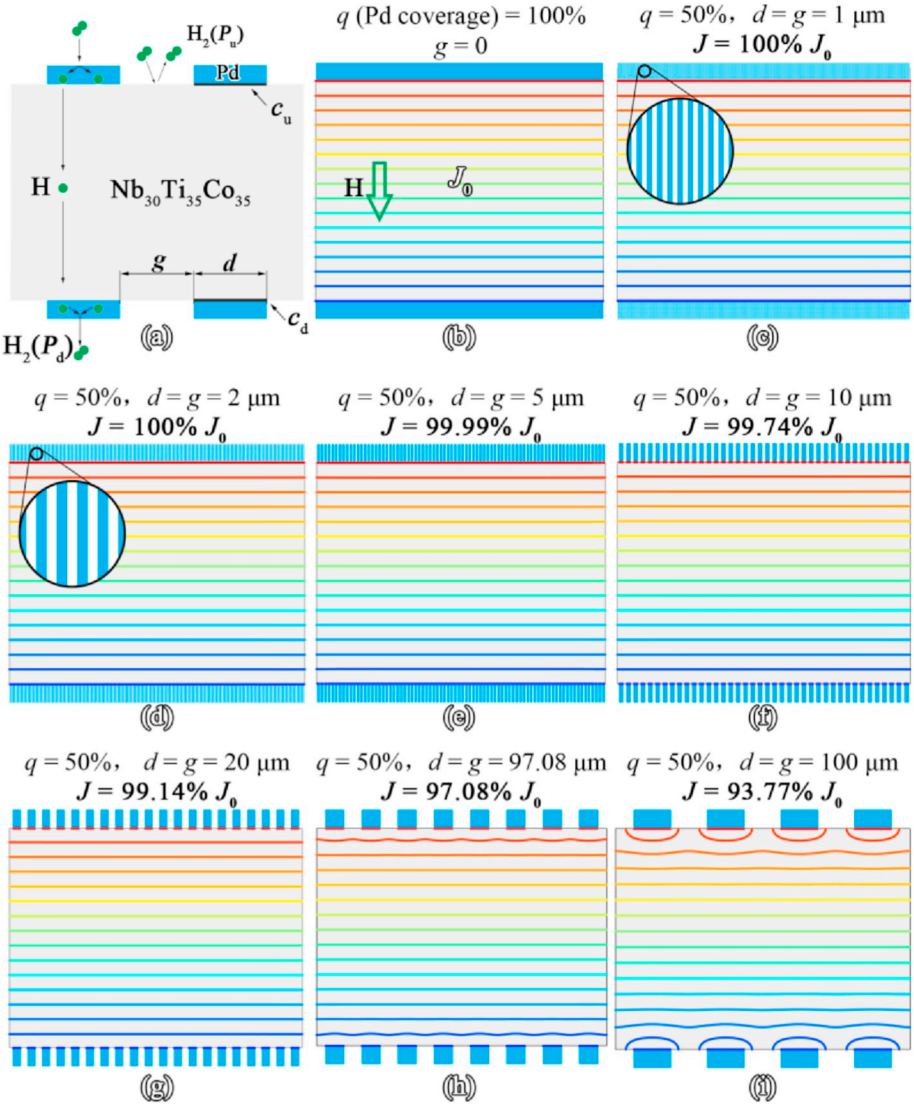

Fig. 6. Schematics of hydrogen diffusion through the Pd/$Nb_{30}Ti_{35}Co_{35}$/Pd membrane, in which Figs. (b ~ i) illustrate the influence of Pd distribution (coverage ratio, particle diameter d and space between particles g) on the transport of hydrogen through the membrane. The isolines from red to blue stand for the hydrogen concentrations from c_u(=3.5 × 10^4 mol H/m^3) to c_d (=2.0 × 10^4 mol H/m^3) with a constant interval of 1 × 10^4 mol H/m^3. (For interpretation of the references to color in this figure legend, the reader is referred to the Web version of this article.)

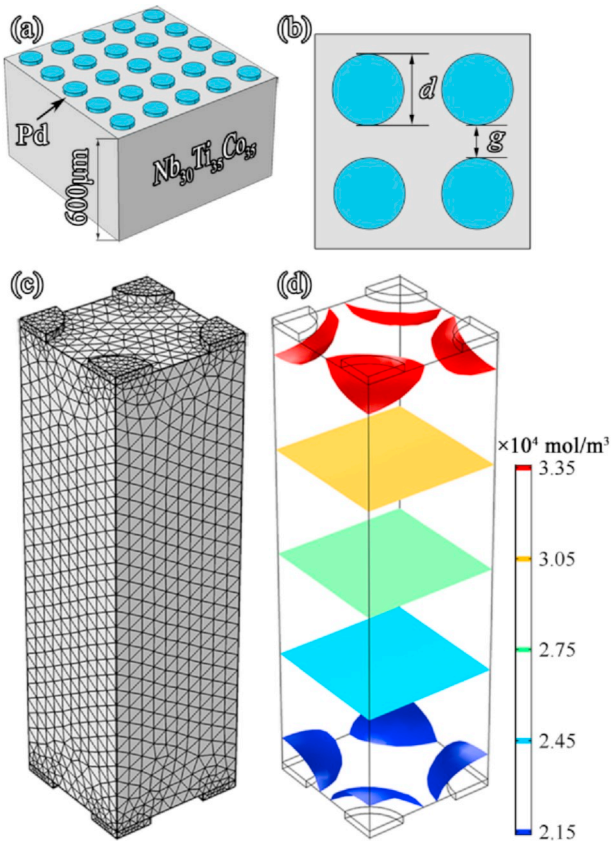

Fig. 7. Schematics of the hydrogen diffusion through the Pd/$Nb_{30}Ti_{35}Co_{35}$/Pd composite membrane. (a) (b) The distribution of the equivalent Pd particles, (c) free tetrahedron meshing, (d) the isosurfaces of hydrogen concentration after the simulation.

concentration from 3.35 to 2.15 × 10^4 mol H/m^3 with a constant interval of 0.3 × 10^4 mol H/m^3. Only after a certain of distance beneath the Pd/$Nb_{30}Ti_{35}Co_{35}$ interface at the upstream side, a flat isosurface perpendicular to the permeation direction is reached. Such distance also exists at the downstream side, and the reduced hydrogen concentration gradient parallel to the permeation direction leads to the reduced hydrogen permeation flux. This distance varies with different distribution modes of the Pd particles. For example, for the same Pd particle diameter, the distance increases with the increasing gap between the Pd particles, resulting in reduced hydrogen permeation flux through the membrane. This is consistent with the 2D modelling, as shown in Fig. 6.

Based on the calculation using COMSOL, the Pd factor (f_{Pd}) is not only dependent on the Pd coverage ratio but also on the size and distribution of Pd particles in the Pd layer. With Pd particle distance falling into the scope from 1 to 100 μm, a non-linear dependence of f_{Pd} on the Pd coverage ratio is found, as shown in Fig. 8(a). When the distance between each two Pd particles is lower than 10 μm, f_{Pd} increases very fast with increasing Pd coverage ratio from 0 to 5% f_{Pd} and becomes higher than 90% at the Pd coverage of 5%. It can reach approximately 100% with a Pd coverage ratio of 30%. When the gap is higher than 5 μm, the increasing tendency of f_{Pd} becomes slower with increasing Pd coverage and it may not reach 100%. In the present work, during the hydrogen permeation test at 400 and 450 °C, the size of the Pd particles is normally 1–2 μm with the gap far below 1 μm (Fig. 3) and the Pd coverage ratio is higher than 70%. Based on Fig. 8(a), f_{Pd} is as high as 100%, indicating that the Pd surface morphology change does not lead to hydrogen flux degradation. The hydrogen flux decline at 450 °C mainly comes from the formation of the boundary layer resulting from interdiffusion between the Pd layer and the $Nb_{30}Ti_{35}Co_{35}$ substrate. However, with a small diameter of Pd particles, for example below 5 μm, with the particle gap (g) of several micrometers (>5 μm), increasing gap leads to fast drop of f_{Pd} and fast and big decline of hydrogen permeation flux, as shown in Fig. 8(b) and (c). This is consistent with the fast decline of hydrogen flux at 550–650 °C, when fast loss of the Pd surface layer (i.e. fast increase in particle gap) occurred as a result of the diffusion between Pd and $Nb_{30}Ti_{35}Co_{35}$ and the peeling of Pd layer.

According to the experimental results (Fig. 3), the diameter of the Pd particles (d) during the hydrogen permeation test is normally about 1 μm. With d about 1 μm, exponential decay of f_{Pd} on the Pd particles gap (g) is proposed based on the simulation results (Fig. 8 (b)):

$$f_{Pd} = \exp\left(-\frac{g}{A}\right) \tag{10}$$

where g is the real-time average distance between Pd particles, and A is the parameters based on the fitting of the simulation results.

The loss of the Pd layer, i.e. the formation of the gap between the Pd particles and its further propagation, comes from the diffusion of Pd into the $Nb_{30}Ti_{35}Co_{35}$ substrate and the peeling of Pd layers. According to the experimental observation, the gap between the Pd particles (g) varies in a wide scope, even in one membrane from a certain permeation process. It is not straightforward to figure out the dependence of g on time based on the experimental results. By correlating the experimental hydrogen flux during permeation tests, an exponential increase of g on operating duration, t, is used:

$$g = g_0\left[\exp\left(\frac{t}{\tau_1}\right) - 1\right] \tag{11}$$

where g_0 and τ_1 are the constants based on the fitting of experimental data.

Combining the effects of the aggregation of the Pd layer and of the boundary layer at the Pd/$Nb_{30}Ti_{35}Co_{35}$ interface, the degradation of the hydrogen flux can be expressed as follows:

$$\frac{J}{J_0} = f_b(t)\cdot f_{Pd}(t) = \frac{1}{1+\beta\cdot\sqrt{t}}\exp\left\{\alpha\cdot\left[1-\exp\left(\frac{t}{\tau_1}\right)\right]\right\} \tag{12}$$

Combining the experimental hydrogen flux curves (Fig. 2) and Eq. (12), the factors such as α, β and τ1 can be obtained, as listed in Table 1.

Based on Table 1, the two factors, $f_b(t)$ and $f_{Pd}(t)$, of the Pd/$Nb_{30}Ti_{35}Co_{35}$/Pd composite membrane during hydrogen permeation tests at 450–650 °C are illustrated in Fig. 9(a). At 450 °C, $f_{Pd}(t)$ is constant as 100%, and the hydrogen flux degradation is induced by low hydrogen permeability of the boundary layer, i.e. $f_b(t)$. At 500 °C, slight decrease of $f_{Pd}(t)$ occurs with test duration up to 150 h, and the hydrogen decline mainly comes from the decrease in $f_b(t)$. At temperatures from 550 to 650 °C, a fast drop in $f_b(t)$ occurs at the beginning, leading to the first step of hydrogen flux decline at these temperatures. As to $f_{Pd}(t)$, after a slight decrease from the beginning, a fast reduction of $f_{Pd}(t)$ occurs beyond a critical operating duration, which contributes to the second fast decline of hydrogen flux and the final null hydrogen flux. This is consistent with the experimental observation at 500–650 °C.

In conclusion, the degradation of the Pd/$Nb_{30}Ti_{35}Co_{35}$/Pd membrane during hydrogen permeation tests at 450–650 °C comes from the deterioration of the Pd catalytic layer and the formation of the low hydrogen permeable boundary layer as a result of interdiffusion. It is not straightforward to prevent the aggregation/peeling of the Pd layer at relatively high temperatures. Developing a new catalytic layer other than Pd has been proposed for group 5 hydrogen permeation alloys, for example, the carbide/metal composites [36,37]. However, relatively low hydrogen dissociation rate of carbide/metal composites is an obstacle, which needs to be solved. Increasing application temperature above 600 °C will lead to enhanced catalytic efficiency of carbide/metal composites is considered as a promising strategy for future practical application. Hence, using carbide/metal catalytic layer may become a potential solution for hydrogen permeable membranes for high application temperatures (>600 °C). In the present work, the hydrogen flux

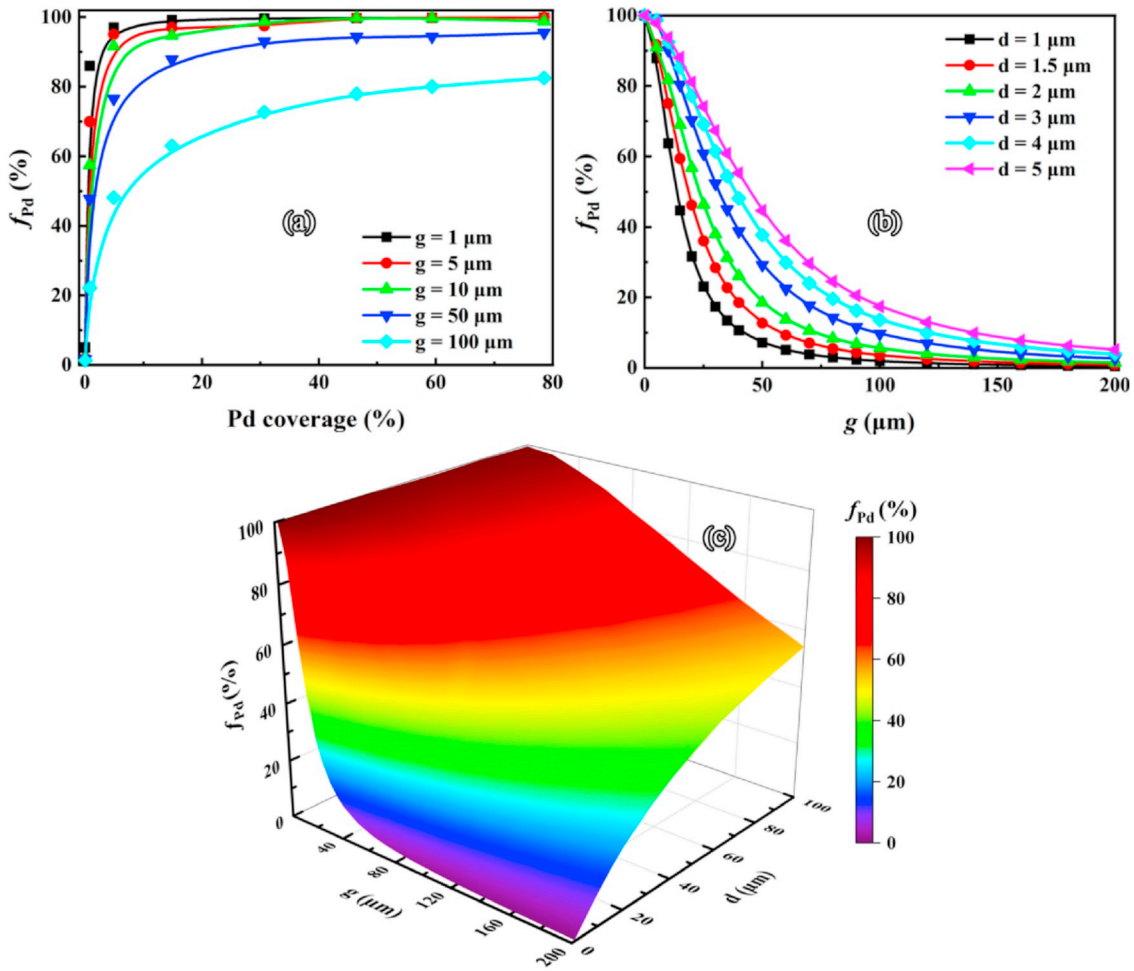

Fig. 8. Dependence of Pd factor f_{Pd} on the distribution and coverage ratio of Pd particle. The values of d and g fall into the range of actual experimental results (1–200 μm). (a) f_{Pd} ~ Pd coverage; (b) f_{Pd} ~ g; (c) f_{Pd} ~(g, d).

Table 1
Factors of the numerical description of the permeation flux degradation.

Temperature (°C)	J_0 (10^{-3} mol H_2 $m^{-2}s^{-1}$)	τ_1 (h)	α	β
450	25	8.83 × 10^8	760	8.11 × 10^{-3}
500	35	1.65 × 10^3	234	0.13
550	44	13.9	1.18 × 10^{-3}	1.02
600	59	6.0	1.29 × 10^{-5}	1.94
650	89	3.22	1.45 × 10^{-7}	8.71

degradation at 450 °C is induced by the formation of the boundary layer as a result of the interdiffusion between the Pd and $Nb_{30}Ti_{35}Co_{35}$. For avoiding the interdiffusion between Pd and the substrate material and the resulting degradation or failure, an intermediate diffusion barrier layer such as an oxide layer, in between was proposed [38,39]. This however needs a much thicker Pd coating layer, for example 25 μm in thickness, which is similar to the thickness of Pd-based membranes. The overall thickness of the membrane and the intermediate oxide layer finally lead to a reduced hydrogen permeation rate. Recent work by Jeon et al. [40] demonstrates that grain boundary segregation strategy during the design of group 5 alloys can help hinder the fast diffusion of Pd along the grain boundaries and thus contributes to improved stability of the membrane.

4. Conclusions

Degradation of hydrogen flux through the Pd/$Nb_{30}Ti_{35}Co_{35}$/Pd composite membrane at operating temperatures above 400 °C was experimentally and theoretically investigated. The microstructural change concerning both the aggregation of the Pd particles in the catalytic Pd layer and the formation of the barrier layer between the Pd surface layer and $Nb_{30}Ti_{35}Co_{35}$ substrate was characterized. The degradation mechanism of the hydrogen flux depends on the operating temperature. The degradation at operating temperatures at 450 °C is mainly induced by the formation of the boundary layer, which contributes to the fast declination of hydrogen flux from the beginning of the permeation process. With operating temperature from 500 to 650 °C, in combination with the formation of the boundary layer, the aggregation of the catalytic Pd layer led to the two-step degradation of hydrogen flux and fast decline to nil hydrogen flux.

Declaration of competing interests

The authors declare that they have no known competing financial interests or personal relationships that could have appeared to influence the work reported in this paper.

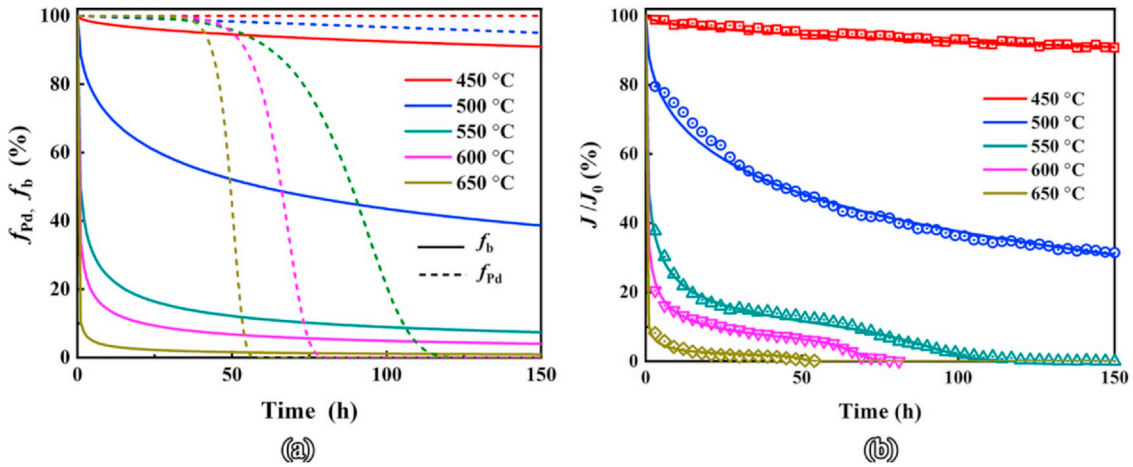

Fig. 9. Calculated degradation of the hydrogen flux through the Pd/$Nb_{30}Ti_{35}Co_{35}$/Pd membrane (a) in different circumstances and (b) the fitting based on the numerical description.

CRediT authorship contribution statement

Xiao Liang: Investigation, Data curation, Writing - original draft. **Xinzhong Li:** Conceptualization, Funding acquisition, Methodology, Resources, Supervision, Writing - review & editing, Project administration. **Hiromi Nagaumi:** Writing - review & editing. **Jingjie Guo:** Writing - review & editing. **Fausto Gallucci:** Resources, Writing - review & editing. **Martin van Sint Annaland:** Resources, Writing - review & editing. **Dongmei Liu:** Conceptualization, Supervision, Writing - review & editing.

Acknowledgments

This project was supported by the National Natural Science Foundation of China (Grants Nos. 51771066, 51571075 and 51274077) and the program of China Scholarships Council.

Appendix

The steady state hydrogen flux through the Pd/$Nb_{30}Ti_{35}Co_{35}$/Pd composite membrane can be described as follows:

$$J = \frac{P_u^{0.5} - P_d^{0.5}}{\sum_i \frac{l_i}{K_i D_i}} \tag{A1}$$

where.

P_u is the hydrogen pressure at the upstream surface,
P_d is the hydrogen pressure at the downstream surface,
l_i is the thickness of i-layer,
K_i is the hydrogen solubility constant of i-layer,
D_i is the hydrogen diffusion coefficient of i-layer.

When the Pd catalytic layer is compact and there is no boundary layer between the Pd layer and the $Nb_{30}Ti_{35}Co_{35}$ substrate,

$$\sum_i \frac{l_i}{K_i D_i} = \left(\frac{l_{Pd}}{K_{Pd} D_{Pd}}\right)_u + \frac{l_{Nb}}{K_{Nb} D_{Nb}} + \left(\frac{l_{Pd}}{K_{Pd} D_{Pd}}\right)_d \tag{A2}$$

where.

l_{Pd} is the initial thickness of Pd catalytic layer, which is 1 μm,
l_{Nb} is the initial thickness of $Nb_{30}Ti_{35}Co_{35}$ layer, which is 600 μm,
K_{Pd} is the hydrogen solubility constant of Pd catalytic layer,
K_{Nb} is the hydrogen solubility constant of $Nb_{30}Ti_{35}Co_{35}$ layer,
D_{Pd} is the hydrogen diffusion coefficient of Pd catalytic layer,
D_{Nb} is the hydrogen diffusion coefficient of $Nb_{30}Ti_{35}Co_{35}$ layer,
"u" and "d" refer to the upstream and downstream sides respectively.

Combining Eqs. A1 and A2, the hydrogen flux at the beginning the permeation test is

$$J = \frac{P_u^{0.5} - P_d^{0.5}}{\sum_i \frac{l_i}{K_i D_i}} = \frac{P_u^{0.5} - P_d^{0.5}}{\frac{2l_{Pd}}{K_{Pd} D_{Pd}} + \frac{l_{Nb}}{K_{Nb} D_{Nb}}} \tag{A3}$$

The hydrogen permeability ($\Phi = K{\cdot}D$) of $Nb_{30}Ti_{35}Co_{35}$ at 400 °C is 2.7 times that of pure Pd. Considering that the thickness of the Pd catalytic layer is only 1 μm, which is far less than that of $Nb_{30}Ti_{35}Co_{35}$ (600 μm), Eq. (A3) can be simplified as following:

$$J = \frac{P_u^{0.5} - P_d^{0.5}}{\frac{l_{Nb}}{K_{Nb}D_{Nb}}} \tag{A4}$$

When a new layer forms at the Pd/$Nb_{30}Ti_{35}Co_{35}$ boundary due to the interdiffusion between Pd and $Nb_{30}Ti_{35}Co_{35}$ at high temperatures,

$$\sum_i \frac{l_i}{K_i D_i} = \left(\frac{l_{Pd} - \frac{l_b}{2}}{K_{Pd}D_{Pd}}\right)_u + \left(\frac{l_b}{K_b D_b}\right)_u + \frac{l_{Nb} - l_b}{K_{Nb}D_{Nb}} + \left(\frac{l_b}{K_b D_b}\right)_d + \left(\frac{l_{Pd}}{K_{Pd}D_{Pd}}\right)_d \tag{A5}$$

where.

l_b is the thickness of the boundary layer formed between the Pd layer and the $Nb_{30}Ti_{35}Co_{35}$ layer,
K_b is the hydrogen solubility constant of the boundary layer formed between the Pd layer and the $Nb_{30}Ti_{35}Co_{35}$ layer,
D_b is the hydrogen diffusivity of the boundary layer formed between the Pd layer and the $Nb_{30}Ti_{35}Co_{35}$ layer.

Similarly, the hydrogen flux after the formation of the boundary layer can be simplified as following:

$$J = \frac{P_u^{0.5} - P_d^{0.5}}{\frac{l_{Nb} - l_b}{K_{Nb}D_{Nb}} + \frac{2l_b}{K_b D_b}} \tag{A6}$$

According to the experimental observation, the thickness of the boundary layer is normally less than 5 μm. Hence, Eq. (A6) can be simplified as:

$$\begin{aligned} J &= \frac{P_u^{0.5} - P_d^{0.5}}{\frac{l_{Nb}}{K_{Nb}D_{Nb}} + \frac{2l_b}{K_b D_b}} \\ &= \frac{P_u^{0.5} - P_d^{0.5}}{\frac{l_{Nb}}{K_{Nb}D_{Nb}}} \times \frac{1}{1 + \frac{2l_b}{K_b D_b} \times \frac{K_{Nb}D_{Nb}}{l_{Nb}}} \\ &= J_0 \times \frac{1}{1 + \frac{2l_b}{K_b D_b} \times \frac{K_{Nb}D_{Nb}}{l_{Nb}}} \end{aligned} \tag{A7}$$

Assuming

$$\beta_0 = \frac{2}{K_b D_b} \times \frac{K_{Nb}D_{Nb}}{l_{Nb}} \tag{A8}$$

Eq. (A7) can be changed to

$$J = J_0 \times \frac{1}{1 + \beta_0 l_b} \tag{A9}$$

The thickness of the boundary layer can be calculated as:

$$l_b = \gamma\sqrt{t} \tag{A10}$$

where γ is the coefficient of diffusion couple between Pd and $Nb_{30}Ti_{35}Co_{35}$, and t is time.

Combining Eq. (A9) and (A10),

$$J = J_0 \times \frac{1}{1 + \beta_0\gamma\sqrt{t}} = J_0 \times \frac{1}{1 + \beta\sqrt{t}} \tag{A11}$$

References

[1] J.O. Abe, A.P.I. Popoola, E. Ajenifuja, O.M. Popoola, Hydrogen energy, economy and storage: review and recommendation, Int. J. Hydrogen Energy 44 (2019) 15072–15086.

[2] S.S. Kumar, V. Himabindu, Hydrogen production by PEM water electrolysis – a review, Mater. Sci. Energy. Technol. 2 (2019) 442–454.

[3] B. Anzelmo, J. Wilcox, S. Liguori, Hydrogen production via natural gas steam reforming in a Pd-Au membrane reactor. Comparison between methane and natural gas steam reforming reactions, J. Membr. Sci. 568 (2018) 113–120.

[4] N.A. Al-Mufachi, S. Nayebossadri, J.D. Speight, W. Bujalski, R. Steinberger-Wilckens, D. Book, Effects of thin film Pd deposition on the hydrogen permeability of $Pd_{60}Cu_{40}$ wt% alloy membranes, J. Membr. Sci. 493 (2015) 580–588.

[5] C. Acar, I. Dincer, Review and evaluation of hydrogen production options for better environment, J. Clean. Prod. 218 (2019) 835–849.

[6] F. Gallucci, E. Fernandez, P. Corengia, M. van Sint Annaland, Recent advances on membranes and membrane reactors for hydrogen production, Chem. Eng. Sci. 92 (2013) 40–66.

[7] J.M. Silva, L.S. Ribeiro, J.J.M. Órfão, S. Tosti, M.A. Soria, L.M. Madeira, From sorption-enhanced reactor to sorption-enhanced membrane reactor: a step towards H_2 production optimization through glycerol steam reforming, Chem. Eng. J. 368 (2019) 795–811.

[8] A.A. Plazaola, D.A. Pacheco Tanaka, M. Van Sint Annaland, F. Gallucci, Recent advances in Pd-based membranes for membrane reactors, Molecules 22 (2017) 51.

[9] J. Liu, S. Bellini, N.C.A. de Nooijer, Y. Sun, D.A. Pacheco Tanaka, C. Tang, H. Li, F. Gallucci, A. Caravella, Hydrogen permeation and stability in ultra-thin PdRu supported membranes, Int. J. Hydrogen Energy (2019), https://doi.org/10.1016/j.ijhydene.2019.03.212.

[10] M. Incelli, A. Santucci, S. Tosti, F. Mallozzi, M. Sansovini, F. Marini, Design and first experimental results of a new multi-tube Pd-Ag membrane module, Fusion Eng. Des. 146 (2019) 2729–2733.

[11] M. Catti, O. Fabelo, A. Filabozzi, A. Pietropaolo, A. Santucci, S. Tosti, Kinetics of deuteration of the $Pd_{0.772}Ag_{0.228}$ alloy with α/β phase transition by in-situ neutron diffraction, J. Alloy. Compd 790 (2019) 502–508.
[12] Y. Nakamura, H. Yukawa, A. Suzuki, T. Nambu, Y. Matsumoto, Y. Murata, Alloying effects on hydrogen permeability of V without catalytic Pd overlayer, J. Alloys Compd. 645 (2015) S275–S279.
[13] K. Ishikawa, Y. Saeki, Y. Miyajima, T. Watanuki, A. Machida, Effects of rolling and annealing on hydrogen permeability and crystal orientation in Nb-TiNi two-phase alloys, Int. J. Hydrogen Energy 44 (2019) 23101–23106.
[14] W. Luo, K. Ishikawa, K. Aoki, Hydrogen permeable Ta–Ti–Ni duplex phase alloys with high resistance to hydrogen embrittlement, J. Alloys Compd. 460 (2008) 353–356.
[15] H. Yukawa, C. Tsukada, T. Nambu, Y. Matsumoto, Hydrogen solubility and permeability of V–W–Mo alloy membrane for hydrogen separation and purification, J. Alloys Compd. 580 (2013) S386–S390.
[16] X. Li, F. Huang, D. Liu, X. Liang, R. Chen, M. Rettenmayr, Y. Su, J. Guo, H. Fu, V-Cr-Cu dual-phase alloy membranes for hydrogen separation: an excellent combination of ductility, hydrogen permeability and embrittlement resistance, J. Membr. Sci. 524 (2017) 354–361.
[17] S.A. Wassie, J.A. Medrano, A. Zaabout, S. Cloete, J. Melendez, D.A.P. Tanaka, S. Amini, M. van Sint Annaland, F. Gallucci, Hydrogen production with integrated CO_2 capture in a membrane assisted gas switching reforming reactor: proof-of-Concept, Int. J. Hydrogen Energy 43 (2018) 6177–6190.
[18] J.A. Medrano, I. Potdar, J. Melendez, V. Spallina, D.A. Pacheco-Tanaka, M. van Sint Annaland, F. Gallucci, The membrane-assisted chemical looping reforming concept for efficient H_2 production with inherent CO_2 capture: experimental demonstration and model validation, Appl. Energy 215 (2018) 75–86.
[19] E. Fernandez, J.A. Medrano, J. Melendez, M. Parco, J.L. Viviente, M. van Sint Annaland, F. Gallucci, D.A. Pacheco Tanaka, Preparation and characterization of metallic supported thin Pd–Ag membranes for hydrogen separation, Chem. Eng. J. 305 (2016) 182–190.
[20] T.F. Fuerst, Z. Zhang, A.M. Hentges, S.-T.B. Lundin, C.A. Wolden, J.D. Way, Fabrication and operational considerations of hydrogen permeable Mo_2C/V metal membranes and improvement with application of Pd, J. Membr. Sci. 549 (2018) 559–566.
[21] T. Nozaki, Y. Hatano, Hydrogen permeation through a Pd/Ta composite membrane with a HfN intermediate layer, Int. J. Hydrogen Energy 38 (2013) 11983–11987.
[22] F. Ren, W. Yin, Q. Yu, X. Jia, Z. Zhao, B. Wang, Solution and diffusion of hydrogen isotopes in tungsten-rhenium alloy, J. Nucl. Mater. 491 (2017) 206–212.
[23] E. Yan, H. Huang, S. Sun, Y. Zou, H. Chu, L. Sun, Development of Nb-Ti-Co alloy for high-performance hydrogen separating membrane, J. Membr. Sci. 565 (2018) 411–424.
[24] X. Li, X. Liang, D. Liu, R. Chen, M. Rettenmayr, Y. Su, J. Guo, H. Fu, Microstructure dependent hydrogen permeability in eutectic $Nb_{30}Ti_{35}Co_{35}$, Int. J. Hydrogen Energy 41 (2016) 13086–13092.
[25] K. Hashi, K. Ishikawa, T. Matsuda, K. Aoki, Microstructure and hydrogen permeability in Nb–Ti–Co multiphase alloys, J. Alloy Compd. 425 (2006) 284–290.
[26] D. Liu, X. Li, H. Geng, R. Chen, M. Rettenmayr, Y. Su, H. Li, J. Guo, H. Fu, Development of $Nb_{35}Mo_5Ti_{30}Ni_{30}$ alloy membrane for hydrogen separation applications, J. Membr. Sci. 553 (2018) 171–179.
[27] M.D. Dolan, Non-Pd BCC alloy membranes for industrial hydrogen separation, J. Membr. Sci. 362 (2010) 12–28.
[28] A.A. Kodentsov, G.F. Bastin, F.J.J. van Loo, Chapter six - application of diffusion couples in phase diagram determination, in: J.C. Zhao (Ed.), Methods for Phase Diagram Determination, Elsevier Science Ltd, Oxford, 2007, pp. 222–245.
[29] M. Watanabe, Z. Horita, M. Nemoto, Observations of diffusion-couple interfaces in Ni-Al system, defect diffus, Forum 143–147 (1997) 637–642.
[30] T. Yamada, K. Miura, M. Kajihara, N. Kurokawa, K. Sakamoto, Formation of intermetallic compound layers in Sn/Au/Sn diffusion couple during annealing at 433 K, J. Mater. Sci. 39 (2004) 2327–2334.
[31] H. Keller, Temperature aging of external connections condensation soldered to Ti-Pd-Au thin films, IEEE Trans. Compon., Hybrids, Manuf. Technol. 2 (1979) 180–195.
[32] V.N. Alimov, Y. Hatano, A.O. Busnyuk, D.A. Livshits, M.E. Notkin, A.I. Livshits, Hydrogen permeation through the Pd–Nb–Pd composite membrane: surface effects and thermal degradation, Int. J. Hydrogen Energy 36 (2011) 7737–7746.
[33] X. Li, X. Liang, D. Liu, R. Chen, M. Rettenmayr, Y. Su, J. Guo, H. Fu, Microstructural stability and its effect on hydrogen permeability in equiaxed and directionally solidified eutectic $Nb_{30}Ti_{35}Co_{35}$ alloys, Int. J. Hydrogen Energy 40 (2015) 9026–9031.
[34] B.D. Morreale, M.V. Ciocco, R.M. Enick, B.I. Morsi, B.H. Howard, A.V. Cugini, K. S. Rothenberger, The permeability of hydrogen in bulk palladium at elevated temperatures and pressures, J. Membr. Sci. 212 (2003) 87–97.
[35] T.L. Ward, T. Dao, Model of hydrogen permeation behavior in palladium membranes, J. Membr. Sci. 153 (1999) 211–231.
[36] S.K. Gade, S.J. Chmelka, S. Parks, J.D. Way, C.A. Wolden, Dense carbide/metal composite membranes for hydrogen separations without platinum group metals, Adv. Mater. 23 (2011) 3585–3589.
[37] J.Y. Han, C.H. Kim, H. Lim, K.Y. Lee, S.K. Ryi, Diffusion barrier coating using a newly developed blowing coating method for a thermally stable Pd membrane deposited on porous stainless-steel support, Int. J. Hydrogen Energy 42 (2017) 12310–12319.
[38] D. Edlund, D. Friesen, B. Johnson, W. Pledger, Hydrogen-permeable metal membranes for high-temperature gas separations, Gas Separ. Purif. 8 (1994) 131–136.
[39] D.J. Edlund, J. McCarthy, The relationship between intermetallic diffusion and flux decline in composite-metal membranes: implications for achieving long membrane lifetime, J. Membr. Sci. 107 (1995) 147–153.
[40] W.S. Ko, J.Y. Oh, J.H. Shim, J.Y. Suh, W.Y. Yoon, B.J. Lee, Design of sustainable V-based hydrogen separation membranes based on grain boundary segregation, Int. J. Hydrogen Energy 39 (2014) 12031–12044.